water

MDPI

Article

Differences in Reference Evapotranspiration Variation and Climate-Driven Patterns in Different Altitudes of the Qinghai–Tibet Plateau (1961–2017)

Yuan Liu, Xiaolei Yao, Qianyang Wang, Jingshan Yu *, Qi Jiang, Weiwei Jiang and Luyi Li

College of Water Sciences, Beijing Normal University, Beijing 100875, China; 201921470018@mail.bnu.edu.cn (Y.L.); yaoxiaolei87@163.com (X.Y.); 201931470001@mail.bnu.edu.cn (Q.W.); 201821470010@mail.bnu.edu.cn (Q.J.); 201631470011@mail.bnu.edu.cn (W.J.); 201821470015@mail.bnu.edu.cn (L.L.)

* Correspondence: jingshan@bnu.edu.cn; Tel.: +86-10-58807814

Abstract: Reference evapotranspiration (ET_0) in the hydrological cycle is one of the processes that is significantly affected by climate change. The Qinghai–Tibet Plateau (QTP) is universally recognized as a region that is sensitive to climate change. In this study, an area elevation curve is used to divide the study area into three elevation zones: low (below 2800 m), medium (2800–3800 m) and high (3800–5000 m). The cumulative anomaly curve, Mann–Kendall test, moving t-test and Yamamoto test results show that a descending mutation occurred in the 1980s, and an ascending mutation occurred in 2005. Moreover, a delay effect on the descending mutation in addition to an enhancement effect on the ascending mutation of the annual ET_0 were coincident with the increasing altitude below 5000 m. The annual ET_0 series for the QTP and different elevation zones showed an increasing trend from 1961 to 2017 and increased more significantly with the increase in elevation. Path analysis showed that the climate-driven patterns in different elevation zones are quite different. However, after the ascending mutations occurred in 2005, the maximum air temperature (Tmax) became the common dominant driving factor for the whole region and the three elevation zones.

Keywords: ET_0; mutation analysis; temporal trend; path analysis; climate driving factor

Citation: Liu, Y.; Yao, X.; Wang, Q.; Yu, J.; Jiang, Q.; Jiang, W.; Li, L. Differences in Reference Evapotranspiration Variation and Climate-Driven Patterns in Different Altitudes of the Qinghai–Tibet Plateau (1961–2017). *Water* **2021**, *13*, 1749. https://doi.org/10.3390/w13131749

Academic Editors: Roberto Ranzi and Kazimierz Banasik

Received: 25 April 2021
Accepted: 22 June 2021
Published: 24 June 2021

1. Introduction

Rapid global climate change has had a vast impact on the ecological environment and biological living systems [1,2]. Changes in water resources and water demand are among the important signals of climate change [3–6]. As the most active factor of the water cycle, evapotranspiration is not only the unique junction of the water transport and energy cycle in the earth-atmospheric system but also a hydrological cycle process, which is significantly affected by climate change [7–10]. As a result of the unfeasibility of the direct prediction of evapotranspiration, people usually estimate the reference evapotranspiration (ET_0) first when formulating crop irrigation plans [11]. ET_0 is a metric that refers to the maximum evaporation that can be achieved by a fixed underlying surface when the water supply is sufficient, as defined by the Food and Agriculture Organization of the United Nations (FAO) [12]. ET_0 is one of the important indicators to reflect the regional evapotranspiration capacity and crop water requirement [13]. The change of ET_0 is only related to climate factors and location. Studying the changing trend of ET_0 plays an essential role in the calculation of the water balance in a watershed when developing crop irrigation plans and drought warning [14–17].

Climate change has significantly changed the spatial–temporal patterns of reference evapotranspiration in many regions [18–23]. Since the 1960s, the increasing global temperature has resulted in an obvious change in the trend of reference evapotranspiration in different regions of the world [24–27]. In recent years, the annual series of ET_0 showed a

significant increasing trend in the Amazon basin, Kazakhstan, Romania and the Ecuador coast [24–27]; however, a decreased ET_0 appears in many other regions around the world, such as the Qilian Mountains, the Huaihe River Basin, the upper reaches of the Yellow River, and a major part of Northern China [28–35]. The abovementioned phenomenon is called "the evaporation paradox". Xing et al. [36] found that this was due to the limitation of relative humidity. Furthermore, relative humidity is the main driving factor of ET_0 change in Tunisia, the Loess Plateau, Sichuan Plateau, Guangxi Basin, Yunnan Guizhou Plateau and many other regions of China [37–40]. It has also been found that wind speed is the dominant variable in the Huaihe River Basin and Southwest China [34,41]. McVicar et al. [29] concluded that the decrease in ET_0 was mainly related to aerodynamic factors (the global wide performance of wind speed decline) and relative humidity (the significant humidity increase in the warm season in Australia, Central and Southern Canada) at the global scale. In addition, radiation composition, temperature and pollutant concentration were also discovered to be key factors motivating the change of ET_0 [42–44]. Because different regions respond to climate change quite differently, it is necessary to conduct regional research. Moreover, most of the relevant research at present focuses on the change trends and its impact factors, only a few people have studied the impact relationships between these factors.

Liu et al. [45] found that regions with a higher altitude are more sensitive to climate change. As the most sensitive and vulnerable region in the context of global environmental change, the warming rate of the Qinghai–Tibet Plateau (QTP) is significantly higher than other parts of the world during the same period [9,45–47]. A large number of studies have shown that the dramatic warming of the QTP has led to the rapid degradation of glaciers and subsequently strengthened the hydrological cycle process and the hydraulic connectivity in this region [48–51]. Furthermore, Huang et al. [52] suggested that compared with human factors, climate factors have a greater impact on vegetation dynamics in the QTP. Climate warming leads to the degradation of alpine grassland and changes the soil nutrients as well as the components of the alpine grassland ecosystem, which has a strong impact on the productivity of the plant community and soil microbial community [53–58]. In addition to being a significant characteristic of climate change, ET_0 is also an important index of crop water demand and a key referential factor of the hydrological cycle. Consequently, the analysis of the ET_0 changing trend and climate-driven mode of the QTP is not only of great value as a reference for guiding regional agricultural activity and investigating the structure of the ecosystem, but also of great significance for monitoring the dynamic changes of the world's water resource reserves. However, most of the existing research is mainly based on the spatial scale of the whole region of the QTP, ignoring the huge altitude difference in the region.

The objectives of this study are as follows: (1) to identify the temporal variation trend and mutation year of ET_0 at different elevations in the QTP over the past 57 years, (2) to analyze spatial characteristics of ET_0 and its trend, and (3) to explore the driving pattern and influence process between climate factors in different elevation zones on ET_0 change before and after mutation. The results can help people understand the response mechanism of ET_0 to climate change, clarify the complex relationship between multiple climate factors and provide a reference for agricultural and livestock production and water resource management.

2. Materials and Methods

2.1. Study Area and Data

The Qinghai–Tibet Plateau (26°00′ N~39°47′ N, 73°19′ E~104°47′ E), which has a total area of approximately 2.5 million km^2, involving 8 countries (Figure 1), with an average altitude of more than 4000 m, is the plateau with the highest altitude in the world and is known as the "roof of the world" [59]. Furthermore, with approximately 70% of the global alpine permafrost, the QTP is the source of some major Asian rivers, including the Indus, Ganges, Salween, Brahmaputra, Mekong, Irrawaddy, Yangtze and Yellow rivers, known

as "the world water tower" [60–62]. Because of its unique geographical conditions, fragile ecological environment and sensitive climate change, the response of the QTP to climate change is indicative of other regions.

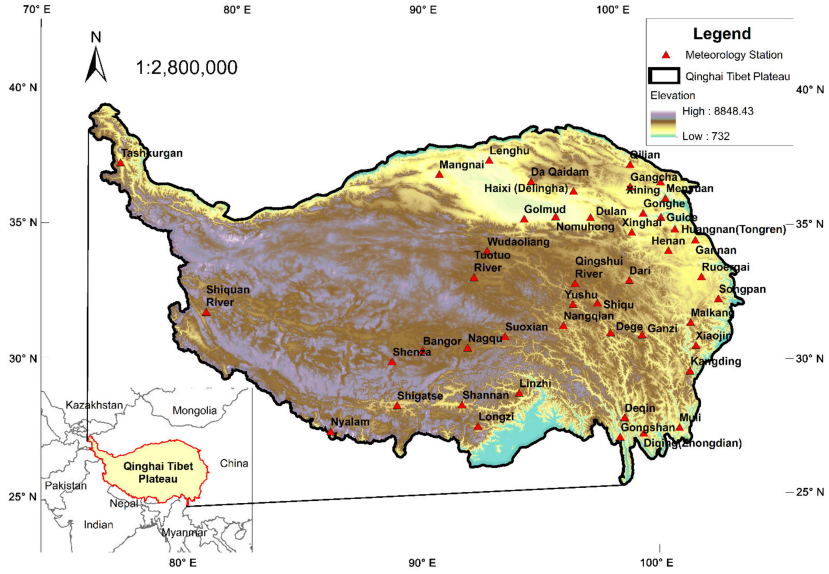

Figure 1. Scope, altitude and geographical location of study area, and distribution of meteorological stations.

The datasets were obtained from the China Meteorological Data Service Center (CMDC) (available online at: http://data.cma.cn/, accessed on 13 April 2020), which have undergone quality control and outlier processing before release (available online at: http://data.cma.cn/, accessed on 13 April 2020). About the few missing data, we interpolate it by the nearest neighbor method. We selected 46 meteorological stations with long-term, relatively continuous and representative data in the QTP (Figure 1). The daily meteorological data from 1961 to 2017 contain eight climatic elements, including daily actual atmospheric pressure (*AP*), mean temperature (*Tmean*), maximum temperature (*Tmax*), minimum temperature (*Tmin*), precipitation (*P*), relative humidity (*RH*), sunshine duration (*SD*) and wind speed (U_2).

The altitude of the QTP ranges from 732 m to 8848.43 m (Figure 1). In this study, the area–elevation curve of the QTP was drawn (Figure 2), and 46 meteorological stations were assigned into three elevation zones (low, medium, and high) according to the curve to analyze the variation trend of ET_0 in different elevation zones in the QTP. Immerzeel et al. [60] used this method to capture the spatial climate heterogeneity in the QTP.

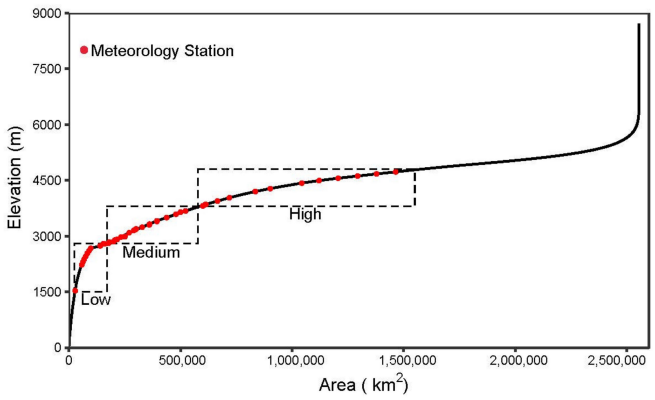

Figure 2. Area-elevation curve for QTP. The dashed boxes are the altitude and area range of the three elevation zones. The altitude of the low-elevation zone ranges from 1500 m to 2800 m (11 stations), the medium is 2800 m to 3800 m (22 stations), and the high is 3800 m to 4800 m (13 stations).

2.2. FAO Penman-Monteith Formula

The Penman–Monteith (P-M) formula is recommended by FAO [12] as the sole standard method to calculate the ET_0, and it is currently one of the most widely used, together with the pan evaporation method and some formulas, in the world [63,64]. In this paper, the P-M formula is used to calculate daily ET_0 values:

$$ET_0 = \frac{0.408\Delta(R_n - G) + \gamma \frac{900}{T_{mean}+273} U_2(e_s - e_a)}{\Delta + \gamma(1 + 0.34U_2)} \quad (1)$$

where Δ is the slope of the relationship curve between saturated water pressure and temperature (kPa $^{\circ}C^{-1}$); R_n is the net radiation on the crop surface (MJ m^{-2}·day^{-1}); G is the soil heat flux (MJ m^{-2}·day^{-1}); γ is the hygrometer constant (kPa $^{\circ}C^{-1}$); T_{mean} is the average air temperature ($^{\circ}C$); U_2 is the wind speed at a height of 2 m above the ground (ms^{-1}); e_s is the air saturation vapor pressure (kPa); e_a is the actual vapor pressure (kPa).

The net radiation is calculated using the following formula:

$$R_n = R_{ns} - R_{nl} \quad (2)$$

$$R_{ns} = (1 - \alpha)R_s \quad (3)$$

$$R_s = \left(a_s + b_s \frac{n}{N}\right) R_a \quad (4)$$

$$R_a = \frac{24(60)}{\pi} G_{sc} d_r [w_s \sin\varphi \sin\theta + \cos\varphi \cos\theta \sin w_s] \quad (5)$$

$$R_{nl} = \sigma \left[\frac{T_{max,k}^4 + T_{min,k}^4}{2}\right] (0.34 - 0.14\sqrt{e_a}) \left(1.35 \frac{R_s}{R_{so}} - 0.35\right) \quad (6)$$

where R_{ns} is the shortwave radiation (MJ m^{-2}·day^{-1}); α is the canopy reflectance of vegetation with a value of 0.23; n is the sunshine duration (h); N is the maximum possible sunshine duration (h); R_a is the solar radiation at the top of the atmosphere (MJ m^{-2}·day^{-1}); G_{sc} is the solar constant with a value of 0.082 (MJ m^{-2} min^{-1}); d_r is the inverse relative distance of Earth–Sun; w_s is the angle of the sunset sun (rad); φ is the latitude (rad); θ is the solar declination (rad); R_{nl} is the net long wave radiation (MJ m^{-2}·day^{-1}); σ is the Stefan–Boltzmann constant, the value is 4.903×10^{-9} (MJ K^{-4} m^{-2} day^{-1}); $T_{max,k}$ is the maximum daily air temperature (K); $T_{min,k}$ is the minimum daily air temperature (K); R_{so} is the value of short wave radiation on the surface of vegetation on sunny days (MJ m^{-2}·day^{-1}). Ye, J.S. et al. [65] found that a_s = 0.24, b_s = 0.6 and $R_{so} = \left(0.64 + 5.48 * 10^{-5} Z\right) R_a$ are suitable for the QTP, where Z is the altitude (m).

2.3. Data Preprocessing

Before trend analysis for ET_0, the Ljung-Box test (LB test) was used to test the autocorrelation of the data, and the Cochrane–Orcutt method was used to transform the variables of the sites with autocorrelation.

The LB test is widely used in white-noise monitoring of time series, especially in the field of meteorology [66,67]. First, assuming that the sequences are completely uncorrelated, this method constructs a statistic Q:

$$Q = n(n+2) \sum_{k=1}^{h} \frac{\rho_k^2}{n-k} \quad (7)$$

where n is the number of the sample, ρ_k^2 is the autocorrelation coefficient of the k-order lag of the sample, and the statistic Q obeys the chi-square distribution. At the α significance level, the reject domain is $Q > x_{1-\alpha,h}^2$. When the p-value of Q (h) is less than α, the original hypothesis is rejected and the sequence receives autocorrelation.

At a 0.05 significance level, this study calculated the *p*-value at the first order lay of the original sequence by the LB test (Table S1 in Supplementary Information). If the sequences with autocorrelation feature, the Cochrane–Orcutt method [68] was used for variable transformation:

$$X_t' = X_t - \rho X_{t-1} \tag{8}$$

$$\rho = \frac{\sum_{i=1}^{n-1}(X_i - \overline{X})(X_{i+1} - \overline{X})}{\sum_{i=1}^{n}(X_i - \overline{X})^2} \tag{9}$$

Execute the LB test again on the new sequence after conversion. If autocorrelation still exists, execute the variable conversion again by Cochrane–Orcutt until autocorrelation is removed. Table S1 (in Supplementary Information) shows the *p*-value of the original sequence and the converted sequence. It can be seen that many sites have autocorrelation, but the autocorrelation can be removed after one conversion.

2.4. Temporal Trend and Mutation Analysis Method

2.4.1. Cumulative Anomaly Curve

A cumulative anomaly curve can intuitively indicate the long-term evolution trend and continuous change of a sequence, and it is a common method to judge the change trend of hydrological and meteorological sequences [69,70]. The calculation procedure of the cumulative anomaly is as follows:

$$\overline{x_t} = \sum_{i=1}^{t}(x_i - \overline{x}), t = 1, 2, 3 \ldots n \tag{10}$$

$$\overline{x} = \frac{1}{n}\sum_{i=1}^{n} x_i, i = 1, 2, 3 \ldots n \tag{11}$$

where x_i is the meteorological dataset, n is the length of the dataset. The anomaly is the distance to the average value, which reflects the degree of data dispersion. The rising of the cumulative anomaly curve showed an upward trend, while the opposite showed a downward trend. Since the mutation point must appear near the peak or inflection point of the cumulative anomaly curve, the mutation year can be roughly tested.

2.4.2. Mann–Kendall Test

Recommended by the WMO, the Mann–Kendall (MK) test is widely used as a non-parametric test of temperature, precipitation and other factors [71]. The advantage is that the samples do not need to follow a certain distribution and are not disturbed by small fluctuations. The MK test can as well reveal the trend and mutation of a dataset [72].

Define two statistics named S and Z, the calculation process is as follows:

$$\mathrm{S} = \sum_{i=1}^{n-1}\sum_{j=i+1}^{n} sgn(x_j - x_i) \tag{12}$$

$$gn(\theta) = \begin{cases} 1, & \text{if } \theta > 0 \\ 0, & \text{if } \theta = 0 \\ -1, & \text{if } \theta < 0 \end{cases} \tag{13}$$

$$\mathrm{Var(s)} = \frac{n(n-1)(2n+5)}{18} \tag{14}$$

$$Z = \begin{cases} \frac{s-1}{\sqrt{var(s)}}, & s > 0 \\ 0, & \theta = 0 \\ \frac{s+1}{\sqrt{var(s)}}, & s < 0 \end{cases} \tag{15}$$

where x_i and x_j are two sequential values of the meteorological dataset ($1 < i < j < n$), n is the length of the dataset; $gn(\theta)$ is a symbolic function; Z is an indicator for the severity of the change trend. The positive value indicates that the trend is rising, while a negative value indicates that the trend is falling. If $|Z| \geq \left|Z_{(1-\alpha)/2}\right|$, it means that at an α significance level, the data series change significantly.

Define d_k as the sum of the cumulative numbers when $x_j > x_i$ ($1 < i < j < n$). The mathematical expectation and variance of d_k are:

$$\mathrm{E}(d_k) = \frac{n(n-1)}{4} \tag{16}$$

$$\mathrm{D}(d_k) = \frac{k(k-1)(2k+5)}{72} \tag{17}$$

$$UF_k = \frac{d_k - \mathrm{E}(d_k)}{\sqrt{\mathrm{D}(d_k)}} \tag{18}$$

where $2 \leq k \leq n$, $UF_1 = 0$; at an α significance level, if $UF_k \geq |U_{\alpha/2}|$, the data series change significantly. UD_k is the negative sequence of UF_k. When the intersection point of the UF_k curve and UD_k curve is within the confidence interval, the point is a mutation point.

2.4.3. Moving T-Test

The moving t-test examines whether the difference between the average values of the two datasets are significant to detect mutations, which is widely used in the study of time series [73]. The calculation method of the statistic t is as follows:

$$\mathrm{t} = \frac{\overline{x_1} - \overline{x_2}}{S\sqrt{\frac{1}{n_1} + \frac{1}{n_2}}} \tag{19}$$

$$\mathrm{S} = \sqrt{\frac{n_1 {S_1}^2 + n_2 {S_2}^2}{n_1 + n_2 - 2}} \tag{20}$$

where x_1 and x_2 are two parts of the datasets, n_1 and n_2 are their lengths, $\overline{x_1}$ and $\overline{x_2}$ are their average values, and S_1 and S_2 are their standard deviations.

The statistic t is submitted to the t-distribution, for which freedom $\mathrm{v} = n_1 + n_2 - 2$. At α significance level, if $\mathrm{t} \geq |t_\alpha|$, the point is a mutation point.

2.4.4. Yamamoto Test

The Yamamoto test defines the signal-to-noise ratio (SNR) of meteorological factors, which is simple, effective and intelligible [74]. Its calculation formula is as follows:

$$\mathrm{SNR} = \frac{|\overline{x_1} - \overline{x_2}|}{S_1 + S_2} \tag{21}$$

Similar to the moving t-test, where x_1 and x_2 are two parts of the datasets, n_1 and n_2 are their lengths, $\overline{x_1}$ and $\overline{x_2}$ are their average values, and S_1 and S_2 are their standard deviations.

If SNR > 1.0, there is a mutation in the point. Furthermore, if SNR > 2.0, it can be considered a strong mutation year.

Since the current methods for identifying mutation points have their own advantages and disadvantages, this study believes that when the results of more than two methods are consistent, specific mutation points are determined.

2.5. Path Analysis

Path analysis is an extension of the multiple linear regression analysis, which can identify and quantify the direct and indirect effects of independent variables on dependent

variables [75]. It is a powerful tool used to analyze the relationship between multiple variables and is widely used in many fields. The analysis process is as follows:

First establish a multiple regression equation:

$$y = b_1x_1 + b_2x_2 + b_3x_3 + \ldots + b_nx_n \tag{22}$$

Then, standardize the variables of Equation (19):

$$\frac{(y-\overline{y})}{\sigma_y} = b_1\frac{\sigma_{x_1}}{\sigma_y} * \frac{(x_1-\overline{x_1})}{\sigma_{x_1}} + b_2\frac{\sigma_{x_2}}{\sigma_y} * \frac{(x_2-\overline{x_2})}{\sigma_{x_2}} + b_3\frac{\sigma_{x_3}}{\sigma_y} * \frac{(x_3-\overline{x_3})}{\sigma_{x_3}} + \ldots + b_n\frac{\sigma_{x_n}}{\sigma_y} * \frac{(x_n-\overline{x_n})}{\sigma_{x_n}} \tag{23}$$

where x_1, x_2, x_3, ... and x_n are different meteorological factors, y is ET_0, $\overline{y}$ is the estimated value obtained by the least squares regression, σ_y is the standard deviation, $\overline{x_i}$ is the estimated value of the independent variable x_i, σ_{x_i} is the standard deviation of x_i, and b_i is a partial regression coefficient. The direct path coefficient P_i is calculated according to the following formula:

$$P_i = b_i\frac{\sigma_{x_i}}{\sigma_y} \tag{24}$$

Establish a path analysis model:

$$r_{i1}P_1 + r_{i2}P_2 + r_{i3}P_3 + \ldots + r_{ij}P_j + \ldots + r_{in}P_n = r_i \tag{25}$$

$$P_e = \sqrt{1 - (r_1P_1 + r_2P_2 + r_3P_3 + \ldots + r_nP_n)} \tag{26}$$

where r_{ij} is the correlation coefficient between x_i and x_j, r_i is the correlation coefficient between x_i and yP_i indicates the direct influence degree of an independent variable on a dependent variable. $r_{ij}P_j$ is the indirect path coefficient, which indicates the indirect influence degree of x_i on y through x_j. P_e indicates the influence of factors not considered by the dependent variables. Figure 3 shows the relationship between variables in path analysis.

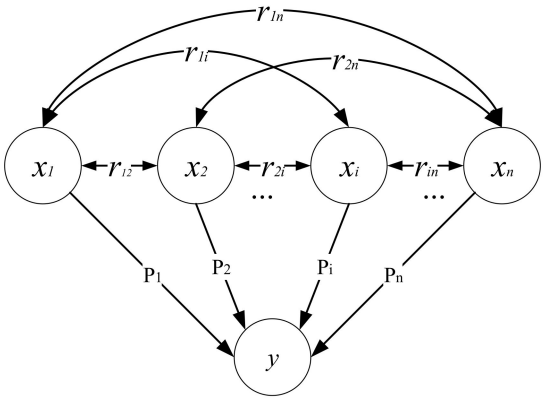

Figure 3. Path network diagram between variables.

In this study, path analysis was used to identify and quantify the direct and indirect effects of the nine climatic elements, including the daily actual atmospheric pressure (*AP*), mean temperature (*Tmean*), maximum temperature (*Tmax*), minimum temperature (*Tmin*), precipitation (*P*), relative humidity (*RH*), sunshine duration (*SD*), wind speed (U_2) and net radiation (R_n) on ET_0.

To realize these methods, we used R programming and the SPSS software. Figure 4 shows the data processing and research procedure of this study.

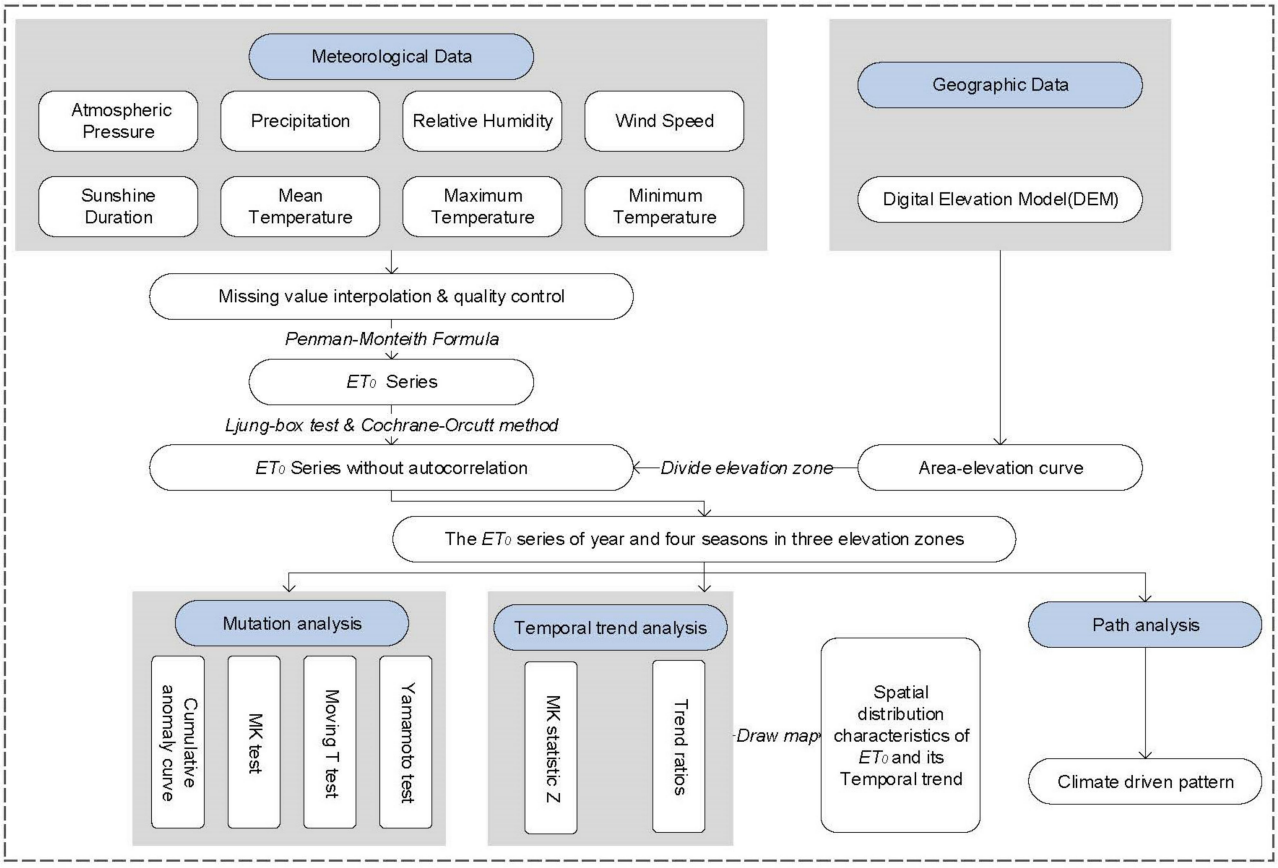

Figure 4. The flowchart of this study.

3. Results and Discussion

3.1. Mutation Analysis of ET_0 in Different Altitudes during 1961–2017

3.1.1. Mutation Analysis of Annual ET_0

The cumulative anomaly curve, Mann–Kendall (MK) test ($\alpha = 0.05$), moving t-test ($\alpha = 0.05$) and Yamamoto test were used to distinguish the mutation year of the ET_0 series annually and for four seasons from 1961 to 2017. Figure 5 shows that there was a turning point from increase to decrease in 1988; nevertheless, a turning point from decrease to increase in the QTP in 1968 and 2005 can be found according to the cumulative anomaly curve. Furthermore, in 1988, the moving t-test curves of the three steps all exceeded the upper critical line, and their SNR reached a peak level. Moreover, the moving t-test and Yamamoto test curves of 5-year and 10-year sliding steps exceeded the critical line in 2005. In addition, the intersection points of the MK curves in the confidence interval were in 1964 and 2012, since the sequences before and after them were relatively short, neither of them can be determined as a true mutation point. In summary, it can be considered that a descending mutation occurred in 1988, while an ascending mutation occurred in 2005 in the QTP.

Figure 5 illustrates that the results of the moving t-test and Yamamoto test in the medium and high-elevation zones were more inclined to 1988 and 2005. Although the positive peak value of the cumulative anomaly curve in the medium-elevation zone was 1981, 1988 was also its inflection point and the decline thereafter became more pronounced. The year 2005 was the negative peak value of the cumulative anomaly curve. Therefore, it can be determined that the descending mutation occurred in 1988, and the ascending mutation occurred in 2005. However, in the low-elevation zone, 1981 was the positive peak of the cumulative anomaly curve and the only intersection of the MK curve in the confidence interval. Both the moving t-test and the Yamamoto test exceeded the critical

line at the point. Therefore, it can be concluded that the descending mutation occurred in 1981. In conclusion, the ET_0 series in the QTP had two mutations during 1961–2017, with a descending mutation occurring in the 1980s and an ascending mutation occurring in 2005. Zhao et al. [76] and Li et al. [77] also found that mutations of climatic factors occurred in China in the 1980s and the early 21st century. Furthermore, with the increase in altitude below 5000 m, the period of the descending mutation of ET_0 was prolonged, and the amplitude of ascending was enhanced.

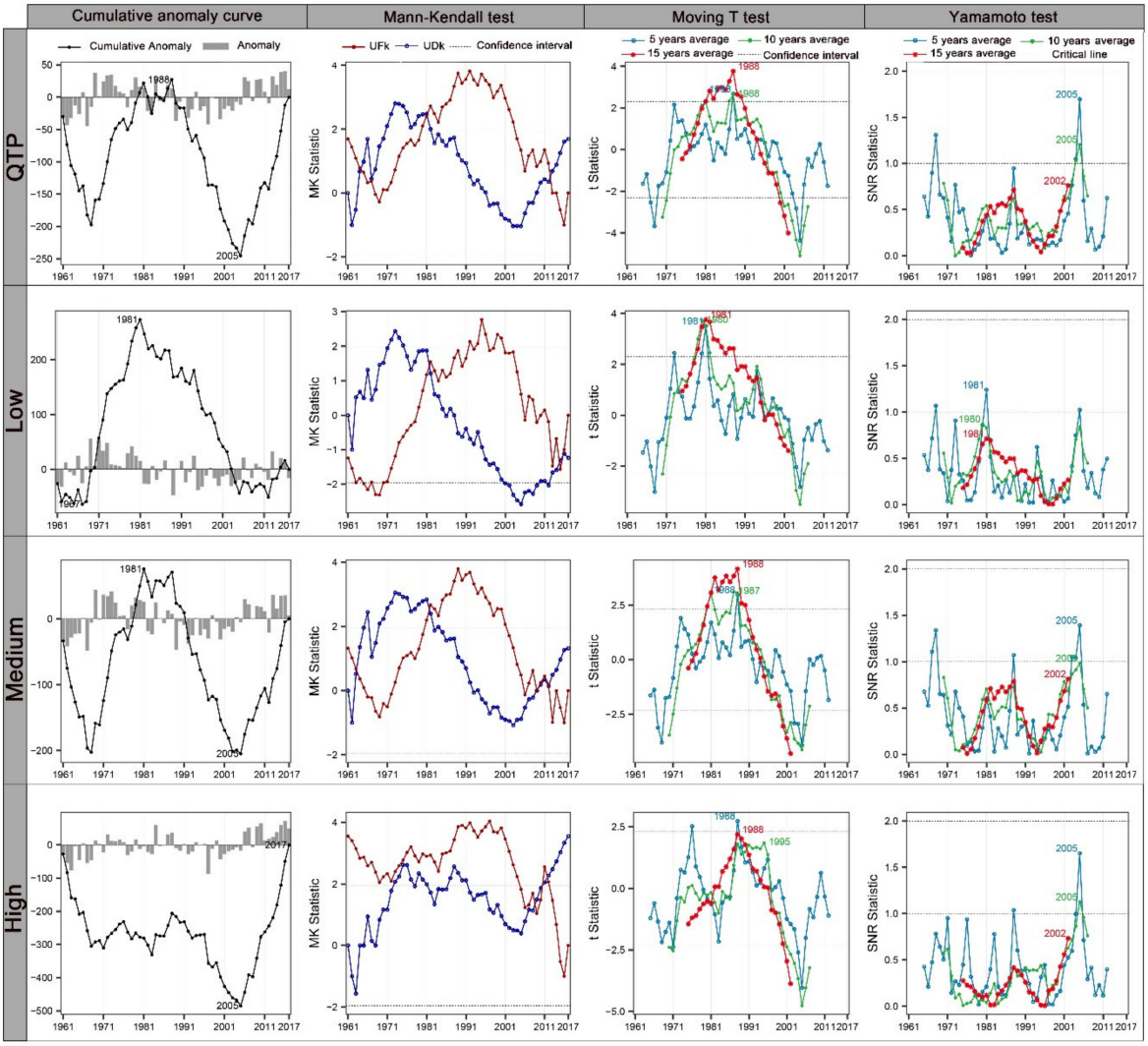

Figure 5. The results of mutation analysis of annual ET_0 on different elevation zones. The marked year of the cumulative anomaly curve is the year in which positive and negative peaks occur. The marks in the moving t-test and Yamamoto test are the years in which the peak value of each line appears.

3.1.2. Mutation Analysis of Four Seasons of ET_0

Figure S1 (in Supplementary Information) shows that the results of the QTP are consistent with the low and the medium-elevation zones in the spring, the descending mutations occurred approximately in 1981, and the ascending mutations occurred in 2005. However, in the high-elevation zone, the peak value of the cumulative anomaly curve was not prominent, the MK curve had more intersections in the confidence interval, and the sliding t-value and SNR value of the three sliding steps did not exceed the critical line, meaning no mutation was detected in the high-elevation zone. Table S2 and Figure S2 (in Supplementary Information) show that in the summer, the descending mutations in the QTP and the medium-elevation zone occurred in 1988–1991 because 1991 was the

intersection point of the MK curve in the confidence interval, and 1988–1991 was the peak segment of their cumulative anomaly curve and passed the moving t-test for the 15-year sliding step. However, in the low-elevation zone, the intersection point of the MK curve in the confidence interval was 1985 and 1987. The other three methods were more inclined to 1981, which can roughly suggest that the descending mutation occurred in 1981–1987. In addition, in the high-elevation zone, the ascending mutations in 2005 were more significant than those in the lower ones. Figure S3 (in Supplementary Information) shows that in autumn, the QTP and the medium-elevation zone had a descending mutation in 1987 and that for the low-elevation zone was in 1994; furthermore, the medium-elevation zone in 2005 showed a significant ascending mutation. Figure S4 (in Supplementary Information) shows that the descending mutation of the winter ET_0 in the QTP, low and medium-elevation zones failed to pass the test since no more than two methods had the same results, and there was an ascending mutation in the high-elevation zone in 2004.

In conclusion, with the increasing altitude below 5000 m, the delay phenomenon of the descending mutation of ET_0 was verified in the summer, and the enhancement effect on the ascending mutation was verified in the summer and winter series.

3.2. Temporal Trend Analysis of ET_0 in Different Altitudes

3.2.1. Temporal Trend of Annual ET_0

The trend ratios and Z-values from the MK test of annual ET_0 in different periods are listed in Table 1 and Table S3. From 1961 to 2017, ET_0 on the QTP showed an increasing trend, which is consistent with the findings of Wang et al. [78], but different from the decreasing trend obtained by Thomas [79] and Kuang and Jiao [80] because the period of the ET_0 series was selected differently. Table 1 also shows that as the altitude increases, the increasing trend of the ET_0 sequence becomes more significant. Before the first mutation, ET_0 in different elevation zones of the QTP showed an increasing trend, and the increasing trend in the low-elevation zone was the most significant by 28.56 mm per decade before 1981. Between the two mutations, there are negative Z-value and change ratios of ET_0 in the QTP, low and high -elevation zones, indicating that their first reduction mutation was a transit mutation, and the middle-elevation zone was a rate or mean value mutation. After the second mutation occurred in 2005, the ET_0 of each elevation zone of the QTP showed an increasing trend, and with the increase in altitude, this trend became more significant, which was consistent with 1961–2017. Thomas [79] also observed the positive relation between evapotranspiration change and station altitude in the mountains of Southwest China.

Table 1. Trend ratios and Z-values from the MK test of annual ET_0 on different elevation zones in different periods.

Region	1961–2017		Before the First Mutation		Between Two Mutations		After the Second Mutation	
	Z	Trend	Z	Trend	Z	Trend	Z	Trend
QTP	1.60	3.31	1.63	11.97	−0.37	−4.06	1.16	15.64
Low	0.47	0.72	2.56 *	28.56	−1.31	−8.45	0.79	10.75
Medium	1.11	2.21	1.58	13.23	0.12	3.16	0.42	12.05
High	3.42 ***	9.84	1.88	17.83	−0.54	−12.77	1.77	32.80

Trend ratios is the slope of linear regression between meteorological factors and year; the slope unit of ET_0 is mm/decade. The three periods before and after the mutation for the QTP, the middle and high-elevation zones are 1961–1987, 1988–2004 and 2005–2017, respectively, and those for the low-elevation zone are 1961–1980, 1981–2004 and 2005–2017, respectively. * Significance levels of 0.05 ($p < 0.05$). *** Significance levels of 0.001 ($p < 0.001$).

3.2.2. Temporal Trend of Four Seasons of ET_0

Figure 6 shows the distribution of the Z-value of ET_0 in the four seasons from the MK test from 1961 to 2017. The graph shows that the change trend of ET_0 varied greatly in different seasons. In winter, the change trend of ET_0 in the whole region was the most consistent, with 89.13% of the stations showing an increasing trend, and 82.93%

of the stations showing a significant increasing trend ($p < 0.05$). Kang et al. [81] and Zhang et al. [82] also concluded that the warming trend in the winter has become more significant. In the spring, the small Z-value bubbles of ET_0 on the stations indicate that the change trend was the gentlest, and the spring ET_0 shows a decreasing trend at the low-elevation stations of 63.64%, while most of the middle and high-elevation zones show an increasing trend, with the proportion of stations being 68.18% and 84.62%. The low elevation zone of the QTP is mainly located in the Qaidam Basin, where the ET_0 decreased significantly in summer and autumn, which is obviously different from the significant increase in other elevation zones.

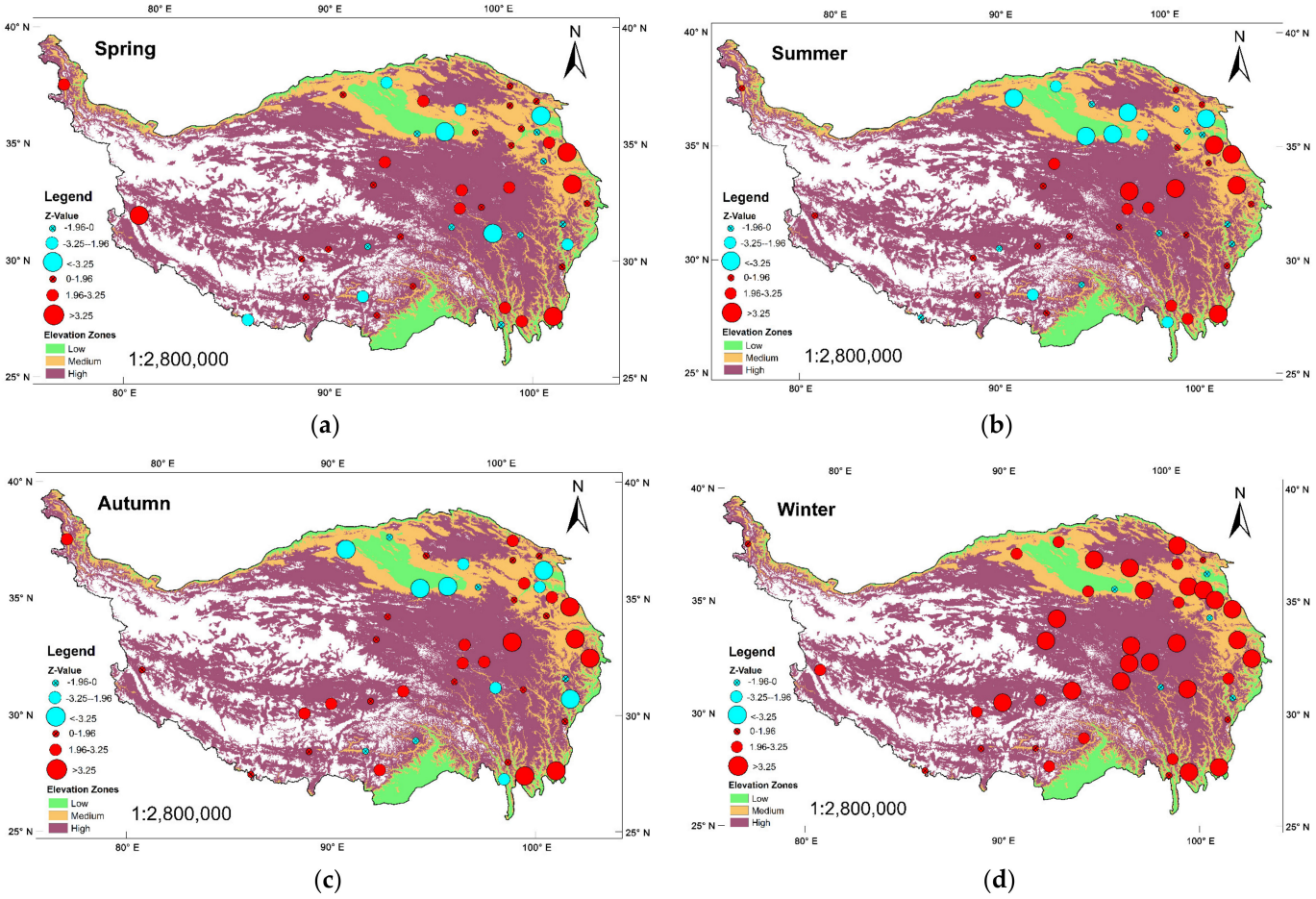

Figure 6. The distribution of the statistical Z-value from the MK test of four seasons (**a**–**d**) at each station of QTP from 1961 to 2017. At $\alpha = 0.05$ significance level, if $|Z| > 1.96$, the ET_0 changes significantly. At $\alpha = 0.001$ significance level, if $|Z| > 3.25$, the ET_0 change is extremely significant. The red bubble represents the increasing trend, the blue represents the decreasing trend, and the larger the bubble is, the more significant the change trend is.

3.3. Climate-Driven Pattern of ET_0 in Different Altitudes

According to the mutation year determined in Section 3.1, the annual ET_0 dataset is divided into three series, which are before the first mutation, between two mutations and after the second mutation. Path analysis was used to quantify the relationship between ET_0 and climate factors. Figure 7 shows that before the first mutation, ET_0 in the QTP was mainly related to the factors, including *Tmean*, U_2, *SD*, *AP* and *Tmax*, of which U_2 and *Tmax* had a strong promotion effect on the change of ET_0, and *AP* directly inhibited ET_0 and indirectly inhibited ET_0 by suppressing wind speed. Moreover, after the descending mutation occurred in 1988, the main climatic factors affecting ET_0 were *Tmax*, U_2 and *Rn*. The direct promotion effect of *Tmax* and U_2 was greatly enhanced. Furthermore, after the

ascending mutation in 2005, the main meteorological factor affecting the change of ET_0 was only *Tmax*, and the combined effect of other factors accounts for only 31.69%.

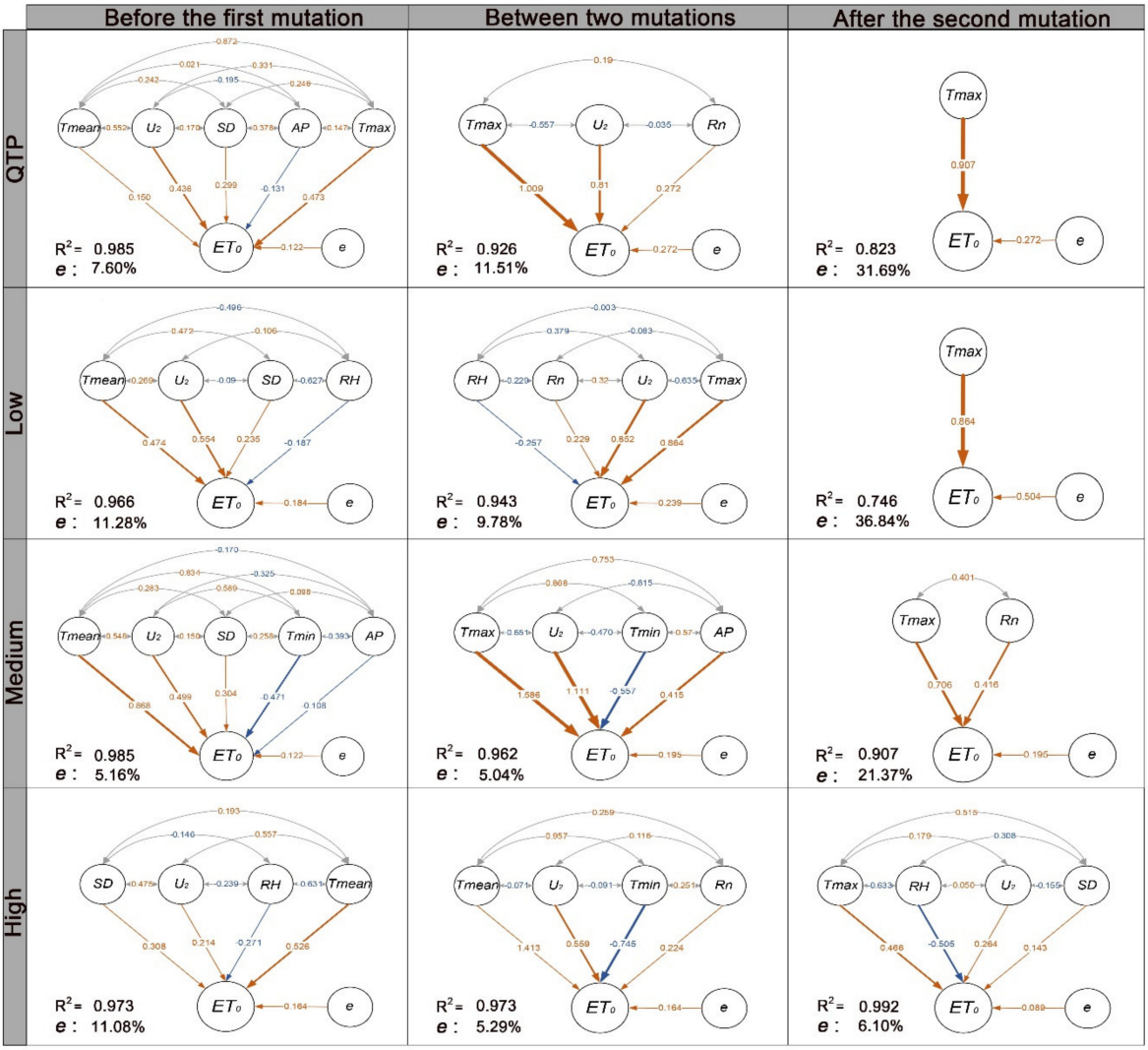

Figure 7. The distribution of the statistical Z-value from the MK test of four seasons at each station of QTP from 1961 to 2017. At $\alpha = 0.05$ significance level, if $|Z| > 1.96$, the ET_0 changes significantly. At $\alpha = 0.001$ significance level, if $|Z| > 3.25$, the ET_0 change is extremely significant. The red bubble represents the increasing trend, the blue represents the decreasing trend, and the larger the bubble is, the more significant the change trend is.

In the low-altitude zone, the main influencing factors were *Tmean*, U_2, *SD* and *RH* before the first mutation, among which the direct promotion of U_2 was the largest, and *RH* directly inhibited ET_0. Liu et al. [41] and Fan and Thomas [39] came to a similar conclusion in China. After the descending mutation occurred in 1981, the main impact factors were *RH*, *Rn*, U_2 and *Tmax*. After 2005, the main impact factors were *Tmax*, with a contribution rate of 63.16%. In the medium-elevation zone, *Tmean*, U_2 and *SD* directly promoted the extent of the change of ET_0, and *Tmin* and *AP* played an inhibitory role before the first mutation. From 1987 to 2004, the direct promotion of *Tmax* and U_2 was greatly enhanced. After 2005, *Tmax* and *Rn* were the main climatic factors, and both contributed. In the high elevation zone, the main climatic factors and driving patterns were consistent with the low-elevation zones before the first mutation. From 1988 to 2004, the direct promotion of *Tmean* and U_2 was enhanced, and *Tmin* had a significant inhibitory effect. After 2005, the main impact factors became *Tmax*, *RH*, U_2 and *SD*.

In general, before the first mutation, *Tmean* and U_2 played a major role in the change of ET_0 in QTP and the three elevation zones. Between the two mutations, the promotion effect of *Tmean* and U_2 in the QTP, low and medium-elevation zones was significantly enhanced, and *Rn* became the main influencing factor in the QTP, low and high-elevation zones. After the ascending mutation occurred in 2005, the direct promotion of *Tmax* in QTP and the three elevation zones contributed the most to the change of ET_0. Zhang et al. [83] also found that *Tmax* had the greatest impact on China's ET_0.

4. Conclusions

Based on the daily meteorological data of 46 meteorological stations in the QTP from 1961 to 2017, the daily ET_0 was calculated by the Penman–Monteith formula. Before trend analysis, we used the Ljung-Box test to verify the autocorrelation of data and used the Cochrane–Orcutt method to transform the variables of the sites with autocorrelation. Furthermore, the cumulative anomaly curve, Mann–Kendall test, moving t-test and Yamamoto test were implemented to identify the mutation year of the ET_0 series in different elevation zones. The combination of the four methods can avoid the error caused by the accidental fluctuation of the sequence and make the recognition results more accurate. In this study, the mutation of the ET_0 series, temporal trend of different elevation zones, and the driving mode of meteorological factors before and after the mutation were explored. The main conclusions are as follows:

(1) The annual and four season ET_0 series in the QTP experienced a descending mutation in the 1980s and an ascending mutation in 2005. The descending mutation of the low-elevation zone (below 2800 m) was in 1981. As the altitude (below 5000 m) increased, the descending mutation of the annual ET_0 tended to be delayed, while the ascending mutation was more significant. The descending mutation of ET_0 in the spring appeared in 1981. The mutation features of the QTP and three elevation zones in the summer were similar to those of the annual scale, but not obvious in winter.

(2) The annual ET_0 series of the Qinghai Tibet Plateau and different elevation zones showed an increasing trend from 1961 to 2017, and it increased more significantly with the increase in elevation below 5000 m. The increasing trend was the most consistent and intense in the winter, with 89.13% of stations showing an increasing trend. Regarding the impact of mutations on trend changes, ET_0 was more prone to mutation of the rate or mean value in the middle-elevation zone, and transit mutation, in which the change trend before and after the mutation is opposite, was more likely to occur in other elevation zones.

(3) Before and after the two mutations, the climate-driven patterns of different elevation zones were quite different, but on the whole, before the descending mutation, the *Tmean* and U_2 played a major role in promoting the change of ET_0 in the QTP and the three elevation zones. Between the two mutations, the promotion effect of *Tmean* and U_2 in the QTP, low and medium-elevation zones was significantly enhanced, and Rn became the main influencing factor in the QTP, low and high-elevation zones. After the ascending mutation occurred in 2005, *Tmax* became the most important driving factor for the QTP and the three elevation zones.

This study explored the different trends of evapotranspiration at different altitudes, which adds new understanding to the regional hydrology research. The results of the study find that there is an increasing trend of reference evapotranspiration in some areas, where the department should conduct drought warning and water resources management to avoid a water shortage. In the future, regional agricultural irrigation plans can be formulated in combination with snow melting or river discharge research.

Supplementary Materials: The following are available online at https://www.mdpi.com/article/10.3390/w13131749/s1, Table S1: The p-value of the raw sequence and the converted sequence by LB test, Figure S1: The results of mutation analysis of spring ET_0 on different elevation zones, Figure S2: The results of mutation analysis of summer ET_0 on different elevation zones, Figure S3: The results of mutation analysis of autumn ET_0 on different elevation zones, Figure S4: The results of mutation analysis of winter ET_0 on different elevation zones, Table S2. The mutation years for ET_0 of four

seasons as a result of Section 3.1.2, Table S3. Z-values from the MK test of ET_0 in four seasons in different elevation zones in different periods.

Author Contributions: Conceptualization, methodology and software, Y.L.; validation, X.Y. and Q.W.; formal analysis and writing—original draft preparation, Y.L. and Q.W.; investigation, L.L.; resources and data curation, W.J. and Q.J.; supervision, project administration and funding acquisition, J.Y. All authors participated in the review and editing. All authors have read and agreed to the published version of the manuscript.

Funding: This study was supported by the National Natural Science Foundation of China (Grant No. 51779007, 41671018) and by the National Key Research and Development Program of China (Grant No. 2016YFC0401308).

Institutional Review Board Statement: Not applicable.

Informed Consent Statement: Not applicable.

Data Availability Statement: Raw datasets are available online at http://data.cma.cn/ accessed on 13 April 2020. Readers can contact the corresponding author for processed data of this study.

Acknowledgments: The authors would like to thank the China Meteorological Data Service Center (CMDC) for providing data.

Conflicts of Interest: The authors declare no conflict of interest.

References

1. Walther, G.-R.; Post, E.; Convey, P.; Menzel, A.; Parmesan, C.; Beebee, T.J.C.; Fromentin, J.-M.; Hoegh-Guldberg, O.; Bairlein, F. Ecological responses to recent climate change. *Nature* **2002**, *416*, 389–395. [CrossRef] [PubMed]
2. Parmesan, C.; Yohe, G. A globally coherent fingerprint of climate change impacts across natural systems. *Nature* **2003**, *421*, 37–42. [CrossRef] [PubMed]
3. Döll, P. Impact of Climate Change and Variability on Irrigation Requirements: A Global Perspective. *Clim. Chang.* **2002**, *54*, 269–293. [CrossRef]
4. Williamson, C.E.; Saros, J.E.; Schindler, D.W. Sentinels of change. *Science* **2009**, *323*, 877–878. [CrossRef] [PubMed]
5. Pritchard, H.D. Asia's shrinking glaciers protect large populations from drought stress. *Nature* **2019**, *569*, 649–654. [CrossRef] [PubMed]
6. Li, X.; Li, Y.; Chen, A.; Gao, M.; Slette, I.; Piao, S. The impact of the 2009/2010 drought on vegetation growth and terrestrial carbon balance in Southwest China. *Agric. For. Meteorol.* **2019**, *269*, 239–248. [CrossRef]
7. Trenberth, K.E.; Fasullo, J.T.; Kiehl, J. Earth's Global Energy Budget. *Bull. Am. Meteorol. Soc.* **2009**, *90*, 311–324. [CrossRef]
8. Jung, M.; Reichstein, M.; Ciais, P.; Seneviratne, S.I.; Sheffield, J.; Goulden, M.L.; Bonan, G.; Cescatti, A.; Chen, J.; De Jeu, R.; et al. Recent decline in the global land evapotranspiration trend due to limited moisture supply. *Nature* **2010**, *467*, 951–954. [CrossRef]
9. Wang, W.; Li, J.; Yu, Z.; Ding, Y.; Xing, W.; Lu, W. Satellite retrieval of actual evapotranspiration in the Tibetan Plateau: Components partitioning, multidecadal trends and dominated factors identifying. *J. Hydrol.* **2018**, *559*, 471–485. [CrossRef]
10. Zhang, Q.; Yang, Z.; Hao, X.; Yue, P. Conversion features of evapotranspiration responding to climate warming in transitional climate regions in northern China. *Clim. Dyn.* **2018**, *52*, 3891–3903. [CrossRef]
11. Howes, D.J.; Fox, P.; Hutton, P. Evapotranspiration from Natural Vegetation in the Central Valley of California: Monthly Grass Reference-Based Vegetation Coefficients and the Dual Crop Coefficient Approach. *J. Hydrol. Eng.* **2015**, *20*, 04015004. [CrossRef]
12. Testa, G.; Gresta, F.; Cosentino, S. Dry matter and qualitative characteristics of alfalfa as affected by harvest times and soil water content. *Eur. J. Agron.* **2011**, *34*, 144–152. [CrossRef]
13. Maček, U.; Bezak, N.; Šraj, M. Reference evapotranspiration changes in Slovenia, Europe. *Agric. For. Meteorol.* **2018**, *260*, 183–192. [CrossRef]
14. Perera, K.C.; Western, A.W.; Nawarathna, B.; George, B. Forecasting daily reference evapotranspiration for Australia using numerical weather prediction outputs. *Agric. For. Meteorol.* **2014**, *194*, 50–63. [CrossRef]
15. Cook, B.I.; Smerdon, J.E.; Seager, R.; Coats, S. Global warming and 21st century drying. *Clim. Dyn.* **2014**, *43*, 2607–2627. [CrossRef]
16. Wu, D.; Fang, S.; Li, X.; He, D.; Zhu, Y.; Yang, Z.; Xu, J.; Wu, Y. Spatial-temporal variation in irrigation water requirement for the winter wheat-summer maize rotation system since the 1980s on the North China Plain. *Agric. Water Manag.* **2019**, *214*, 78–86. [CrossRef]
17. Wurster, P.; Maneta, M.; Beguería, S.; Cobourn, K.; Maxwell, B.; Silverman, N.; Ewing, S.; Jensco, K.; Gardner, P.; Kimball, J.; et al. Characterizing the impact of climatic and price anomalies on agrosystems in the northwest United States. *Agric. For. Meteorol.* **2020**, *280*, 107778. [CrossRef]
18. Xu, C.-Y.; Gong, L.; Jiang, T.; Chen, D.; Singh, V. Analysis of spatial distribution and temporal trend of reference evapotranspiration and pan evaporation in Changjiang (Yangtze River) catchment. *J. Hydrol.* **2006**, *327*, 81–93. [CrossRef]

19. Nam, W.-H.; Hong, E.-M.; Choi, J.-Y. Has climate change already affected the spatial distribution and temporal trends of reference evapotranspiration in South Korea? *Agric. Water Manag.* **2015**, *150*, 129–138. [CrossRef]
20. Wang, Z.; Xie, P.; Lai, C.; Chen, X.; Wu, X.; Zeng, Z.; Li, J. Spatiotemporal variability of reference evapotranspiration and contributing climatic factors in China during 1961–2013. *J. Hydrol.* **2017**, *544*, 97–108. [CrossRef]
21. Ye, L.; Shi, K.; Zhang, H.; Xin, Z.; Hu, J.; Zhang, C. Spatio-Temporal Analysis of Drought Indicated by SPEI over Northeastern China. *Water* **2019**, *11*, 908. [CrossRef]
22. Tran, A.P.; Rungee, J.; Faybishenko, B.; Dafflon, B.; Hubbard, S.S. Assessment of Spatiotemporal Variability of Evapotranspiration and Its Governing Factors in a Mountainous Watershed. *Water* **2019**, *11*, 243. [CrossRef]
23. Wang, H.; Xiao, W.; Zhao, Y.; Wang, Y.; Hou, B.; Zhou, Y.; Yang, H.; Zhang, X.; Cui, H. The Spatiotemporal Variability of Evapotranspiration and Its Response to Climate Change and Land Use/Land Cover Change in the Three Gorges Reservoir. *Water* **2019**, *11*, 1739. [CrossRef]
24. Cavalcante, R.B.L.; Pontes, P.R.M.; Souza-Filho, P.W.M.; de Souza, E. Opposite Effects of Climate and Land Use Changes on the Annual Water Balance in the Amazon Arc of Deforestation. *Water Resour. Res.* **2019**, *55*, 3092–3106. [CrossRef]
25. Hu, Z.; Chen, X.; Chen, D.; Li, J.; Wang, S.; Zhou, Q.; Yin, G.; Guo, M. "Dry gets drier, wet gets wetter": A case study over the arid regions of central Asia. *Int. J. Clim.* **2018**, *39*, 1072–1091. [CrossRef]
26. Prăvălie, R.; Sîrodoev, I.; Patriche, C.; Roșca, B.; Piticar, A.; Bandoc, G.; Sfîcă, L.; Tişcovschi, A.; Dumitrascu, M.; Chifiriuc, C.; et al. The impact of climate change on agricultural productivity in Romania. A country-scale assessment based on the relationship between climatic water balance and maize yields in recent decades. *Agric. Syst.* **2020**, *179*, 102767. [CrossRef]
27. Vera, J.F.R.; Mera, Y.E.Z.; Pérez-Martín, M. Adapting water resources systems to climate change in tropical areas: Ecuadorian coast. *Sci. Total. Environ.* **2020**, *703*, 135554. [CrossRef] [PubMed]
28. Dobson, D.; Meredith, P.; Boon, S.A. Simulation of Subduction Zone Seismicity by Dehydration of Serpentine. *Science* **2002**, *298*, 1407–1410. [CrossRef]
29. McVicar, T.; Roderick, M.L.; Donohue, R.J.; Li, L.T.; Van Niel, T.; Thomas, A.; Grieser, J.; Jhajharia, D.; Himri, Y.; Mahowald, N.M.; et al. Global review and synthesis of trends in observed terrestrial near-surface wind speeds: Implications for evaporation. *J. Hydrol.* **2012**, *416–417*, 182–205. [CrossRef]
30. Zhao, J.; Zhang, Y.; Qian, Y.; Pan, Z.; Zhu, Y.; Zhang, Y.; Guo, J.; Xu, L. Coincidence of variation in potato yield and climate in northern China. *Sci. Total. Environ.* **2016**, *573*, 965–973. [CrossRef]
31. Lin, P.; He, Z.; Du, J.; Chen, L.; Zhu, X.; Li, J. Impacts of climate change on reference evapotranspiration in the Qilian Mountains of China: Historical trends and projected changes. *Int. J. Clim.* **2018**, *38*, 2980–2993. [CrossRef]
32. Li, Y.; Yao, N.; Chau, H.W. Influences of removing linear and nonlinear trends from climatic variables on temporal variations of annual reference crop evapotranspiration in Xinjiang, China. *Sci. Total. Environ.* **2017**, *592*, 680–692. [CrossRef] [PubMed]
33. Xu, S.; Yu, Z.; Yang, C.; Ji, X.; Zhang, K. Trends in evapotranspiration and their responses to climate change and vegetation greening over the upper reaches of the Yellow River Basin. *Agric. For. Meteorol.* **2018**, *263*, 118–129. [CrossRef]
34. Li, M.; Chu, R.; Shen, S.; Islam, A.R.M.T. Dynamic analysis of pan evaporation variations in the Huai River Basin, a climate transition zone in eastern China. *Sci. Total. Environ.* **2018**, *625*, 496–509. [CrossRef] [PubMed]
35. Yang, L.; Feng, Q.; Adamowski, J.F.; Yin, Z.; Wen, X.; Wu, M.; Jia, B.; Hao, Q. Spatio-temporal variation of reference evapotranspiration in northwest China based on CORDEX-EA. *Atmos. Res.* **2020**, *238*, 104868. [CrossRef]
36. Xing, W.; Wang, W.; Shao, Q.; Yu, Z.; Yang, T.; Fu, J. Periodic fluctuation of reference evapotranspiration during the past five decades: Does Evaporation Paradox really exist in China? *Sci. Rep.* **2016**, *6*, 39503. [CrossRef]
37. Baccour, H.; Slimani, M.; Cudennec, C. Structures spatiales de l'évapotranspiration de référence et des variables climatiques corrélées en Tunisie. *Hydrol. Sci. J.* **2012**, *57*, 818–829. [CrossRef]
38. Li, C.; Wu, P.; Li, X.; Zhou, T.; Sun, S.; Wang, Y.; Luan, X.; Yu, X. Spatial and temporal evolution of climatic factors and its impacts on potential evapotranspiration in Loess Plateau of Northern Shaanxi, China. *Sci. Total. Environ.* **2017**, *589*, 165–172. [CrossRef]
39. Fan, Z.-X.; Thomas, A. Decadal changes of reference crop evapotranspiration attribution: Spatial and temporal variability over China 1960–2011. *J. Hydrol.* **2018**, *560*, 461–470. [CrossRef]
40. Jiang, S.; Liang, C.; Cui, N.; Zhao, L.; Du, T.; Hu, X.; Feng, Y.; Guan, J.; Feng, Y. Impacts of climatic variables on reference evapotranspiration during growing season in Southwest China. *Agric. Water Manag.* **2019**, *216*, 365–378. [CrossRef]
41. Liu, T.; Li, L.; Lai, J.; Liu, C.; Zhuang, W. Reference evapotranspiration change and its sensitivity to climate variables in southwest China. *Theor. Appl. Clim.* **2015**, *125*, 499–508. [CrossRef]
42. Gao, Z.; He, J.; Dong, K.; Li, X. Trends in reference evapotranspiration and their causative factors in the West Liao River basin, China. *Agric. For. Meteorol.* **2017**, *232*, 106–117. [CrossRef]
43. Yao, L. Causative impact of air pollution on evapotranspiration in the North China Plain. *Environ. Res.* **2017**, *158*, 436–442. [CrossRef]
44. Zhao, Z.; Wang, H.; Wang, C.; Li, W.; Chen, H.; Deng, C. Changes in reference evapotranspiration over Northwest China from 1957 to 2018: Variation characteristics, cause analysis and relationships with atmospheric circulation. *Agric. Water Manag.* **2020**, *231*, 105958. [CrossRef]
45. Yao, T.; Liu, X.; Wang, N.; Shi, Y. Amplitude of climatic changes in Qinghai-Tibetan Plateau. *Chin. Sci. Bull.* **2000**, *45*, 1236–1243. [CrossRef]
46. Duan, A.; Xiao, Z. Does the climate warming hiatus exist over the Tibetan Plateau? *Sci. Rep.* **2015**, *5*, 13711. [CrossRef]

47. Gao, Q.; Guo, Y.; Xu, H.; Ganjurjav, H.; Li, Y.; Wan, Y.; Qin, X.; Ma, X.; Liu, S. Climate change and its impacts on vegetation distribution and net primary productivity of the alpine ecosystem in the Qinghai-Tibetan Plateau. *Sci. Total. Environ.* **2016**, *554–555*, 34–41. [CrossRef]
48. Zhao, R.; Li, Z.-W.; Feng, G.-C.; Wang, Q.-J.; Hu, J. Monitoring surface deformation over permafrost with an improved SBAS-InSAR algorithm: With emphasis on climatic factors modeling. *Remote Sens. Environ.* **2016**, *184*, 276–287. [CrossRef]
49. Zhang, G.; Yao, T.; Shum, C.K.; Yi, S.; Yang, K.; Xie, H.; Feng, W.; Bolch, T.; Wang, L.; Behrangi, A.; et al. Lake volume and groundwater storage variations in Tibetan Plateau's endorheic basin. *Geophys. Res. Lett.* **2017**, *44*, 5550–5560. [CrossRef]
50. Ran, Y.; Li, X.; Cheng, G. Climate warming over the past half century has led to thermal degradation of permafrost on the Qinghai–Tibet Plateau. *Cryosphere* **2018**, *12*, 595–608. [CrossRef]
51. Zhou, Y.; Li, Z.; Li, J.; Zhao, R.; Ding, X. Glacier mass balance in the Qinghai–Tibet Plateau and its surroundings from the mid-1970s to 2000 based on Hexagon KH-9 and SRTM DEMs. *Remote Sens. Environ.* **2018**, *210*, 96–112. [CrossRef]
52. Huang, K.; Zhang, Y.; Zhu, J.; Liu, Y.; Zu, J.; Zhang, J. The Influences of Climate Change and Human Activities on Vegetation Dynamics in the Qinghai-Tibet Plateau. *Remote Sens.* **2016**, *8*, 876. [CrossRef]
53. Ganjurjav, H.; Gao, Q.; Gornish, E.S.; Schwartz, M.; Liang, Y.; Cao, X.; Zhang, W.; Zhang, Y.; Li, W.; Wan, Y.; et al. Differential response of alpine steppe and alpine meadow to climate warming in the central Qinghai–Tibetan Plateau. *Agric. For. Meteorol.* **2016**, *223*, 233–240. [CrossRef]
54. Chen, Y.-L.; Ding, J.-Z.; Peng, Y.-F.; Li, F.; Yang, G.-B.; Liu, L.; Qin, S.-Q.; Fang, K.; Yang, Y.-H. Patterns and drivers of soil microbial communities in Tibetan alpine and global terrestrial ecosystems. *J. Biogeogr.* **2016**, *43*, 2027–2039. [CrossRef]
55. Zhang, Y.; Dong, S.; Gao, Q.; Liu, S.; Zhou, H.; Ganjurjav, H.; Wang, X. Climate change and human activities altered the diversity and composition of soil microbial community in alpine grasslands of the Qinghai-Tibetan Plateau. *Sci. Total Environ.* **2016**, *562*, 353–363. [CrossRef] [PubMed]
56. Ma, Z.; Liu, H.; Mi, Z.; Zhang, Z.; Wang, Y.; Xu, W.; Jiang, L.; He, J.-S. Climate warming reduces the temporal stability of plant community biomass production. *Nat. Commun.* **2017**, *8*, 15378. [CrossRef]
57. Liu, H.; Mi, Z.; Lin, L.; Wang, Y.; Zhang, Z.; Zhang, F.; Wang, H.; Liu, L.; Zhu, B.; Cao, G.; et al. Shifting plant species composition in response to climate change stabilizes grassland primary production. *Proc. Natl. Acad. Sci. USA* **2018**, *115*, 4051–4056. [CrossRef] [PubMed]
58. Sheng, W.; Zhen, L.; Xiao, Y.; Hu, Y. Ecological and socioeconomic effects of ecological restoration in China's Three Rivers Source Region. *Sci. Total Environ.* **2019**, *650*, 2307–2313. [CrossRef]
59. Luo, D.; Jin, H.; Marchenko, S.S.; Romanovsky, V.E. Difference between near-surface air, land surface and ground surface temperatures and their influences on the frozen ground on the Qinghai-Tibet Plateau. *Geoderma* **2018**, *312*, 74–85. [CrossRef]
60. Xu, X.; Lu, C.; Shi, X.; Gao, S. World water tower: An atmospheric perspective. *Geophys. Res. Lett.* **2008**, *35*. [CrossRef]
61. Immerzeel, W.; Droogers, P.; de Jong, S.; Bierkens, M.F. Large-scale monitoring of snow cover and runoff simulation in Himalayan river basins using remote sensing. *Remote Sens. Environ.* **2009**, *113*, 40–49. [CrossRef]
62. Wang, Y.; Spencer, R.G.M.; Podgorski, D.C.; Kellerman, A.M.; Rashid, H.; Zito, P.; Xiao, W.; Wei, D.; Yang, Y.; Xu, Y. Spatiotemporal transformation of dissolved organic matter along an alpine stream flow path on the Qinghai–Tibet Plateau: Importance of source and permafrost degradation. *Biogeosciences* **2018**, *15*, 6637–6648. [CrossRef]
63. Wang, Z.; Song, W.; Yuan, X.; Yin, L. Spatio-Temporal Variations in Farmland Water Conditions in the Yanhe River Basin. *Water* **2019**, *11*, 2234. [CrossRef]
64. Liu, W.; Liu, L. Analysis of Dry/Wet Variations in the Poyang Lake Basin Using Standardized Precipitation Evapotranspiration Index Based on Two Potential Evapotranspiration Algorithms. *Water* **2019**, *11*, 1380. [CrossRef]
65. Ye, J.; Guo, A.; Sun, G. Statistical Analysis of Reference Evapotranspiration on the Tibetan Plateau. *J. Irrig. Drain. Eng.* **2009**, *135*, 134–140. [CrossRef]
66. Regmi, B.; Lamichhane, S. A dynamic linear model of monthly minimum and maximum temperature changes in three physiographic regions of the Central Himalayas. *Clim. Res.* **2019**, *79*, 1–8. [CrossRef]
67. Drissia, T.K.; Jothiprakash, V.; Anitha, A.B. Statistical classification of streamflow based on flow variability in west flowing rivers of Kerala, India. *Theor. Appl. Clim.* **2018**, *137*, 1643–1658. [CrossRef]
68. Demiroglu, O.C.; Kučerová, J.; Ozcelebi, O. Snow reliability and climate elasticity: Case of a Slovak ski resort. *Tour. Rev.* **2015**, *70*, 1–12. [CrossRef]
69. Peng, D.; Qiu, L.; Fang, J.; Zhang, Z. Quantification of Climate Changes and Human Activities That Impact Runoff in the Taihu Lake Basin, China. *Math. Probl. Eng.* **2016**, *2016*, 1–7. [CrossRef]
70. Misra, V.; Bhardwaj, A. Defining the Northeast Monsoon of India. *Mon. Weather Rev.* **2019**, *147*, 791–807. [CrossRef]
71. Hůnová, I.; Bäumelt, V.; Modlík, M. Long-term trends in nitrogen oxides at different types of monitoring stations in the Czech Republic. *Sci. Total Environ.* **2020**, *699*, 134378. [CrossRef]
72. Gocic, M.; Trajkovic, S. Analysis of changes in meteorological variables using Mann-Kendall and Sen's slope estimator statistical tests in Serbia. *Glob. Planet. Chang.* **2013**, *100*, 172–182. [CrossRef]
73. Yang, Q.; Zheng, J.; Zhu, H. Influence of spatiotemporal change of temperature and rainfall on major grain yields in southern Jiangsu Province, China. *Glob. Ecol. Conserv.* **2020**, *21*, e00818. [CrossRef]
74. Zhao, F.F.; Xu, Z.X.; Huang, J.X.; Li, J.Y. Monotonic trend and abrupt changes for major climate variables in the headwater catchment of the Yellow River basin. *Hydrol. Process.* **2008**, *22*, 4587–4599. [CrossRef]

75. Mellios, N.; Moe, S.J.; Laspidou, C. Machine Learning Approaches for Predicting Health Risk of Cyanobacterial Blooms in Northern European Lakes. *Water* **2020**, *12*, 1191. [CrossRef]
76. Zhao, H.; Pan, X.; Wang, Z.; Jiang, S.; Liang, L.; Wang, X.; Wang, X. What were the changing trends of the seasonal and annual aridity indexes in northwestern China during 1961–2015? *Atmos. Res.* **2019**, *222*, 154–162. [CrossRef]
77. Li, X.; Chen, Z.; Wang, L. Analysis of the Spatiotemporal Variation Characteristics of Main Extreme Climate Indices in Sichuan Province of China from 1968 to 2017. *Appl. Ecol. Environ. Res.* **2020**, *18*, 3211–3242. [CrossRef]
78. Wang, Z.; Ye, A.; Wang, L.; Liu, K.; Cheng, L. Spatial and temporal characteristics of reference evapotranspiration and its climatic driving factors over China from 1979–2015. *Agric. Water Manag.* **2019**, *213*, 1096–1108. [CrossRef]
79. Thomas, A. Spatial and temporal characteristics of potential evapotranspiration trends over China. *Int. J. Climatol.* **2000**, *20*, 381–396. [CrossRef]
80. Kuang, X.; Jiao, J.J. Review on climate change on the Tibetan Plateau during the last half century. *J. Geophys. Res. Atmos.* **2016**, *121*, 3979–4007. [CrossRef]
81. Kang, S.; Xu, Y.; You, Q.; Flügel, W.-A.; Pepin, N.; Yao, T. Review of climate and cryospheric change in the Tibetan Plateau. *Environ. Res. Lett.* **2010**, *5*, 015101. [CrossRef]
82. Zhang, G.; Xie, H.; Kang, S.; Yi, D.; Ackley, S.F. Monitoring lake level changes on the Tibetan Plateau using ICESat altimetry data (2003–2009). *Remote Sens. Environ.* **2011**, *115*, 1733–1742. [CrossRef]
83. Zhang, L.; Traore, S.; Cui, Y.; Luo, Y.; Zhu, G.; Liu, B.; Fipps, G.; Karthikeyan, R.; Singh, V. Assessment of spatiotemporal variability of reference evapotranspiration and controlling climate factors over decades in China using geospatial techniques. *Agric. Water Manag.* **2019**, *213*, 499–511. [CrossRef]